

Nonlinear evolution and formation of cosh-Gaussian breathers in cubic-quintic media possessing hump-shaped quintic nonlinearity

Naveen Gupta, Alex A K, and Deepak Kumar

Citation: Chin. Phys. B, 2026, 35 (**8**): 084205. DOI: 10.1088/1674-1056/ae2d3a
http://cpb.iphy.ac.cn; http://iopscience.iop.org/cpb

What follows is a list of articles you may be interested in

Sensitive sensing based on quantum correlation of photons in weak nonlinear regime

Zi-Qiang Yin(尹子强), Zhi-Hao Liu(刘志豪), Jian Tang(唐健), Hui Jing(景辉), and Xun-Wei Xu(徐勋卫)
Chin. Phys. B, 2026, 35 (**7**): 074201. DOI: 10.1088/1674-1056/ae5c71

Nonlinear perturbation of a high-order exceptional point: Skin discrete breathers and the hierarchical power-law scaling

Hui Jiang(江慧), Enhong Cheng(成恩宏), Ziyu Zhou(周子榆), and Li-Jun Lang(郎利君)
Chin. Phys. B, 2023, 32 (**8**): 084203. DOI: 10.1088/1674-1056/accb47

Linear and nonlinear propagation characteristics of multi-Gaussian laser beams

Naveen Gupta and Sandeep Kumar
Chin. Phys. B, 2020, 29 (**11**): 114210. DOI: 10.1088/1674-1056/abb306

Spatiotemporal propagation dynamics of intense optical pulses in loosely confined gas-filled hollow-core fibers

Rui-rui Zhao(赵睿睿), Ding Wang(王丁), Zhi-yuan Huang(黄志远), Yu-xin Leng(冷雨欣), Ru-xin Li(李儒新)
Chin. Phys. B, 2017, 26 (**1**): 014208. DOI: 10.1088/1674-1056/26/1/014208

Spectral broadening induced by intense ultra-short pulse in 4H-SiC crystals

Chun-hua Xu(徐春华), Teng-fei Yan(闫腾飞), Gang Wang(王刚), Wen-jun Wang(王文军), Jing-kui Liang(梁敬魁), Xiao-long Chen(陈小龙)
Chin. Phys. B, 2016, 25 (**6**): 064206. DOI: 10.1088/1674-1056/25/6/064206

Nonlinear evolution and formation of cosh–Gaussian breathers in cubic-quintic media possessing hump-shaped quintic nonlinearity

Naveen Gupta[†], Alex A K, and Deepak Kumar

Lovely Professional University Phagwara, Phagwara 144411, *India*

(Received 6 November 2025; revised manuscript received 28 November 2025; accepted manuscript online 16 December 2025)

We investigate the nonlinear evolution and formation of cosh–Gaussian (ChG) breathers in a nonlinear optical medium characterized by a cubic–quintic (CQ) refractive index profile with a spatially modulated hump-shaped quintic nonlinearity. The study is motivated by the unique intensity structure of ChG beams, which combines hyperbolic cosine and Gaussian features, enabling a rich interplay between diffraction, self-focusing and nonlinear saturation effects. Employing the moment method, we derive a set of evolution equations governing the beam width and axial phase of the laser beam under the influence of the composite nonlinearity. The analysis reveals critical conditions under which the beam undergoes periodic breathing behavior, indicating the formation of robust breather solitons. The presence of the hump-shaped quintic term introduces a localized nonlinear potential that significantly alters the propagation dynamics of the breather.

Keywords: cosh-Gaussian, breathers, moment theory, cubic quintic, self-focusing

PACS: 42.65.–k

DOI: 10.1088/1674-1056/ae2d3a **CSTR:** 32038.14.CPB.ae2d3a

1. Introduction

Understanding the propagation of intense laser beams through nonlinear optical media has long been a subject of scientific and technological interest. This area of research underpins numerous applications, including advanced laser systems,[1] high-capacity optical interconnects,[2] adaptive beam steering platforms,[3] and nonlinear photonic circuits.[4] In contrast to linear propagation, where beams naturally diffract and spread out over distance, nonlinear optical environments allow the medium itself to respond dynamically to the intensity of light. This self-induced modification of the refractive index can guide and shape the beam in unexpected ways, leading to the emergence of spatially localized waveforms known as optical solitons.[5–8] These self-stabilizing structures persist by balancing the dispersive effects of diffraction against the nonlinear refractive modulation of the medium.

Among the variety of spatial solitons that can form in such settings, a particularly fascinating class is that of breathers.[9,10] Rather than maintaining a static profile, these beams exhibit periodic fluctuations in intensity and transverse width as they propagate, yet remain confined and coherent. Their oscillatory nature is a direct consequence of non-stationary balance mechanisms — where transient dominance of either self-focusing[11,12] or spreading leads to cyclical reshaping of the beam. These breathing dynamics open up avenues for real-time tuneability and adaptive control of light fields in nonlinear devices. This makes breathers particularly suitable for contexts where reconfigurable beam properties are beneficial, such as in light-based trapping systems, ultrafast optical modulation and dynamically adjustable waveguides.

Breathing wave structures are not exclusive to optics. Similar pulsating patterns are seen in a variety of physical systems governed by competing effects. These include surface and internal waves in fluids,[13] oscillatory plasma modes,[14] nonlinear excitations in Bose–Einstein condensates,[15] and even propagating instabilities in reaction-diffusion systems.[16] Despite the diversity of these environments, the presence of breather-like states often signals a common thread: an ongoing interplay between localization and dispersion. The recurrence of these dynamics across scientific domains highlights the universality of breathing solitons and the broad relevance of their governing principles.

In optical settings, the formation and persistence of breathers are shaped by the precise interplay between the beam's phase front evolution and the medium's nonlinear response. While third-order (Kerr) nonlinearities often dominate[17–20] beam dynamics at moderate power levels, they become insufficient to capture the full picture when the input intensity increases. Under these conditions, higher-order nonlinearities, particularly of quintic nature, become significant. The fifth-order term typically introduces a saturating or defocusing component, which tempers the otherwise runaway self-focusing induced by the Kerr effect. This dual contribution — focusing from the cubic and defocusing from the quintic response — establishes a richer framework for stable beam propagation, enabling the existence of complex structures such as oscillatory solitons.

[†]Corresponding author. E-mail: naveens222@rediffmail.com

© 2026 Chinese Physical Society and IOP Publishing Ltd. All rights, including for text and data mining, AI training, and similar technologies, are reserved.

Cubic–quintic (CQ) nonlinear media, characterized by this competing nonlinear behavior, have been shown to support a wide spectrum of exotic beam configurations. Of particular interest are structured laser beams, whose tailored intensity distributions influence their interaction with the nonlinear refractive landscape. One such configuration is the cosh–Gaussian (ChG) beam,[21–24] which combines features of hyperbolic cosine and Gaussian profiles to produce a beam with a flatter central peak. This hybrid structure allows for enhanced control over beam localization and energy distribution, which can significantly impact the formation and stability of nonlinear waveforms.

In this work, we investigate the evolution of ChG beams in CQ media where the quintic nonlinearity is not uniform but follows a hump-shaped spatial profile along the propagation axis. These modulated media introduce an additional degree of complexity, enabling spatially dependent nonlinear interactions that influence the breathing dynamics of the beam. Through semi-analytical and numerical modeling, we explore how the structured intensity profile of ChG beams interacts with the longitudinally modulated (hump-shaped) quintic response to give rise to breather-type solitons. Our focus is on identifying the key signatures of this interaction. These insights aim to contribute to the design of advanced nonlinear photonic systems where light fields can be dynamically sculpted by the medium itself.

2. Formation of a spatial breather

Light propagation through nonlinear optical materials is commonly described using the nonlinear Schrödinger equation (NLSE), a simplified framework that arises from Maxwell's equations when specific conditions are applied. This approach models the nonlinear behavior of the medium by integrating its polarization characteristics into the constitutive equations. A foundational premise of this derivation is that the optical wave can be viewed as a rapidly oscillating carrier modulated by a slowly varying envelope. The envelope evolves over spatial and temporal scales much longer than the carrier's wavelength and period, enabling a scale separation that streamlines the analysis of the system's dynamics.[25–27]

In the case of a medium exhibiting CQ nonlinearity, the NLSE takes the form

$$2ik_0\frac{\partial A_0}{\partial z} = \nabla_\perp^2 A_0 + \frac{k_0^2}{n_0^2}(2n_2\left|A_0^2\right| - 2n_4(z)|A_0^4|)A_0. \quad (1)$$

Here, n_0 is the linear index of refraction of the medium, n_2 is the Kerr coefficient associated with $\chi^{(3)}$ nonlinearity, and n_4 is the coefficient of quintic nonlinearity associated with the $\chi^{(5)}$ effect. The dependence of n_2 on $\chi^{(3)}$ and n_4 on $\chi^{(5)}$ can be seen from the relations

$$n_2 = \frac{3}{8}\frac{\chi^{(3)}}{n_0}, \quad n_4 = \frac{5}{16}\frac{\chi^{(5)}}{n_0}.$$

The z dependence of n_4 indicates the axial modulation of quintic nonlinearity.

In Eq. (1), the evolution of the optical field envelope along the longitudinal axis is governed by a term proportional to the first-order derivative with respect to z, modulated by a complex coefficient. This term encapsulates the gradual transformation of the beam's amplitude as it propagates. The inclusion of the imaginary unit signifies the wave-like character of the process. Meanwhile, the transverse Laplacian $\nabla_\perp^2 A_0$ accounts for spatial diffraction, which manifests as lateral spreading of the beam in the transverse plane. The nonlinear optical response is introduced through an intensity-dependent refractive index variation, represented by the terms involving $|A_0|^2$ and $|A_0|^4$, which may vary along the propagation axis. These nonlinearities lead to phenomena such as beam narrowing or expansion, depending on their respective signs and magnitudes. Collectively, the model captures the competition between linear spreading due to diffraction and nonlinear refractive effects that influence the beam's transverse confinement.

In the present study, the axial modulation of quintic nonlinearity has been modeled as

$$n_4(z) = n_4^0 \mathrm{e}^{-a^2(z-d)^2}. \quad (2)$$

That is, quintic nonlinearity is in the form of an axial hump. Here, n_4^0 is the maximum value of the quintic nonlinearity, i.e., it represents the height of the hump, d is the position of the center of the hump and a gives the measure of the width of the hump. As the value of a increases, the width of the hump reduces.

This modulation of quintic nonlinearity of the medium can be engineered through several physical mechanisms. One approach involves spatially varying the material composition or doping concentration during fabrication, creating a longitudinal gradient in the electronic or molecular response that governs the quintic term.[28] Alternatively, externally applied fields, such as temperature gradients, acoustic waves, or electric fields, can dynamically alter the nonlinear susceptibility along the z direction. Another method exploits optical pumping with a spatially shaped beam, which locally excites carrier populations or changes the molecular alignment, thereby modifying the effective n_4.

This hump-shaped axial modulation of quintic nonlinearity plays a crucial role in controlling the dynamics of breathers in nonlinear optical media, offering a wide range of applications in advanced photonic systems. The quintic term, which becomes significant in strongly nonlinear or resonant materials, often leads to instabilities such as beam breakup or collapse at high intensities. However, introducing an axial hump provides a means of locally enhancing and tailoring the nonlinear response to stabilize and manipulate soliton breathing. This controlled modulation enables efficient optical switching

and the realization of all-optical logic gates, where the breather oscillations act as dynamic states for information encoding. In high-power laser systems, the hump arrests collapse and facilitates stable propagation of intense solitons, thus supporting power scaling and robust soliton lasers. Furthermore, the breathing dynamics under quintic modulation enhance nonlinear spectral broadening, making it valuable for supercontinuum generation in broadband light sources for spectroscopy and frequency metrology. The tunability imparted by the hump also enables all-optical control of soliton amplitude, width, and breathing frequency, which is useful for optical memory and temporal pattern formation. At the same time, in photonic crystal fibers and integrated waveguides, this modulation provides soliton trapping, routing, and multiplexing capabilities. Importantly, since breathers serve as precursors to rogue waves, axial hump modulation can either suppress these extreme events for optical safety or deliberately excite them for high-intensity pulse generation.

Due to the nonlinear nature of Eq. (1), the superposition principle no longer holds, and thus wave components do not combine in a simple additive way. Therefore, traditional methods used to solve linear partial differential equations are no longer effective. To better understand how the optical beam evolves under these conditions, a semi-analytical method known as moment theory is used[29–32] in this paper. This approach provides a practical way to capture the essential features of beam behavior without requiring a full exact solution. Rather than attempting to solve the full wave equation in detail, this method concentrates on the evolution of certain integral characteristics of the beam, such as its spatial extent, central location and angular spread. These characteristics, referred to as moments, are derived from the beam's intensity profile and serve a similar role to statistical moments in describing the shape and behavior of a distribution. By analyzing how these global features change during propagation, the moment-based approach offers meaningful insight into nonlinear effects such as beam narrowing, spreading and collapse, all while sidestepping the complexities of fully resolving the governing differential equations.

Moment theory defines the effective beam width of an optical beam as

$$\langle a^2\rangle = \frac{\int_0^\infty A_0 r^2 A_0^* r\,\mathrm{d}r}{\int_0^\infty A_0 A_0 r\,\mathrm{d}r}. \tag{3}$$

The accuracy of the moment method critically relies on the choice of an appropriate ansatz — a presumed beam shape that reflects the dominant characteristics of the actual optical field. This assumed form is defined by adjustable parameters that encode the beam's spatial structure and its evolution along the propagation direction. If the selected ansatz closely approximates the true profile of the beam, the method can provide robust and insightful predictions of its behavior. In the present study, a ChG-type beam profile is employed as the trial function, with its mathematical expression specified as[21,24]

$$A_0(r) = \frac{E_{00}}{f}\,\mathrm{e}^{-\frac{r^2}{2r_0^2 f^2}}\cosh\left(b\frac{r}{r_0 f}\right). \tag{4}$$

In this formulation, E_{00} represents the peak axial intensity, while r_0 denotes the characteristic beam waist, with r being the radial distance from the beam axis. The parameter f serves as a beam width descriptor and, when normalized by r_0, captures the evolution of the beam's radial extent during propagation through the nonlinear medium. In addition, the parameter b, appearing in the hyperbolic cosine term, significantly affects the transverse beam structure. Often referred to as the beam shaping factor, b governs the steepness of the beam edges, modulating how rapidly the intensity diminishes away from the center. The resulting expression can be reformulated as

$$A_0 = \frac{E_{00}}{2f}\,\mathrm{e}^{\frac{b^2}{2}}\left[\mathrm{e}^{-\frac{1}{2}\left(\frac{r}{r_0 f}+b\right)^2} + \mathrm{e}^{-\frac{1}{2}\left(\frac{r}{r_0 f}-b\right)^2}\right]. \tag{5}$$

From this equation, it is evident that the generation of ChG beams can be understood through the coherent superposition of two identical Gaussian beams, laterally displaced in opposite directions along the x-axis. These beams are centered at positions $\left(\frac{b}{2},0\right)$ and $\left(-\frac{b}{2},0\right)$, and when combined in phase, they give rise to an interference pattern closely resembling the intensity profile of a ChG beam. The separation distance b, often referred to as the shape parameter, determines the degree of spatial separation between the two Gaussians and governs the resulting transverse beam structure.

Using Eq. (4) in Eq. (3), one can obtain

$$\langle a^2\rangle = r_0^2 f^2\left(1+b^2\right). \tag{6}$$

Differentiating Eq. (3) w.r.t z and using the value of $\mathrm{d}A_0/\mathrm{d}z$ from Eq. (1), we obtain

$$I_0\frac{\mathrm{d}}{\mathrm{d}z}\langle a^2\rangle = \mathrm{i}\frac{\pi}{k_0}\int_0^\infty r^2\left\{A_0\left(\nabla_\perp^2 A_0^*\right) - \left(\nabla_\perp^2 A_0\right)A_0^*\right\} r\,\mathrm{d}r\,\mathrm{d}\theta, \tag{7}$$

where

$$I_0 = \int_0^\infty A_0 A_0^* r\,\mathrm{d}r. \tag{8}$$

In obtaining Eq. (7), it is assumed that the power of the beam is conserved during its propagation, i.e., $\mathrm{d}I_0/\mathrm{d}z = 0$.

Differentiating Eq. (7) w.r.t z:

$$\begin{aligned}\frac{\mathrm{d}^2}{\mathrm{d}z^2}\langle a^2\rangle \;=\; & \mathrm{i}\frac{\pi}{I_0 k_0}\int_0^\infty r^2\left\{\left(\nabla_\perp^2\frac{\partial A_0^*}{\partial z}\right)A_0 + \left(\nabla_\perp^2 A_0^*\right)\frac{\partial A_0}{\partial z}\right.\\ & \left. - \left(\nabla_\perp^2\frac{\partial A_0}{\partial z}\right)A_0^* - \left(\nabla_\perp^2 A_0\right)\frac{\partial A_0^*}{\partial z}\right\} r\,\mathrm{d}r.\end{aligned} \tag{9}$$

This equation can be simplified as

$$\frac{\mathrm{d}^2}{\mathrm{d}z^2}\langle a^2\rangle \;=\; \mathrm{i}\frac{\pi}{I_0 k_0}\int_0^\infty r^2\frac{\partial}{\partial r}\left[r\left(\frac{\partial A_0}{\partial z}\frac{\partial A_0^*}{\partial r} - \frac{\partial A_0^*}{\partial z}\frac{\partial A_0}{\partial r}\right)\right.$$

$$+r\left(A_0\frac{\partial}{\partial r}\left(\frac{\partial A_0^*}{\partial z}\right)-A_0^*\frac{\partial}{\partial r}\left(\frac{\partial A_0}{\partial z}\right)\right)\Bigg]. \quad (10)$$

Using wave Eq. (1) and making use of the fact that for the ChG laser beam profile, i.e., Eq. (5):

$$|A_0| = 0, \quad (11)$$

$$\left|\frac{\partial A_0}{\partial r}\right| = 0, \quad (12)$$

$$r^n\frac{\partial^m A_0}{\partial r^m} = 0, \quad (13)$$

$$\frac{\mathrm{d}^2}{\mathrm{d}z^2}\langle a^2\rangle = K_1+K_2+K_3+K_4, \quad (14)$$

where

$$K_1 = \int_0^\infty \frac{\partial}{\partial r}\left(r^2\left|\frac{\partial A_0}{\partial r}\right|^2\right)\mathrm{d}r, \quad (15)$$

$$K_2 = -\frac{\pi}{I_0k_0^2}\int_0^\infty \frac{\partial}{\partial r}|A_0|^2\,\mathrm{d}r, \quad (16)$$

$$K_3 = \frac{\pi}{I_0k_0^2}\int_0^\infty r\left(A_0^*\frac{\partial}{\partial r}\left(r\frac{\partial^2 A_0}{\partial r^2}\right)+A_0\frac{\partial}{\partial r}\left(r\frac{\partial^2 A_0^*}{\partial r^2}\right)\right)\mathrm{d}r, \quad (17)$$

$$K_4 = \frac{2\pi}{I_0n_0}\int_0^\infty r^2A_0\frac{\partial\phi}{\partial r}\mathrm{d}r, \quad (18)$$

$$\phi\left(A_0A_0^\star\right) = 2n_2\left|A_0^2\right| - 2n_4(z)|A_0^4|. \quad (19)$$

Using Eq. (12) in Eq. (15), we obtain

$$K_1 = 0. \quad (20)$$

Using Eq. (11) in Eq. (16), we obtain

$$K_2 = \frac{\pi}{I_0k_0^2}\frac{E_{00}^2}{f^2}. \quad (21)$$

Now, using Eq. (13) in Eq. (17), we obtain

$$K_3 = \frac{\pi}{I_0k_0^2}\left[-\frac{E_{00}^2}{f^2}+\int_0^\infty 4r|\nabla_\perp E_0|^2\,\mathrm{d}r\right]. \quad (22)$$

Using Eqs. (15)–(18) in Eq. (14), we obtain

$$\frac{\mathrm{d}^2}{\mathrm{d}z^2}\langle a^2\rangle = \frac{4\pi}{I_0k_0^2}\int_0^\infty r|\nabla_\perp E_0|^2\,\mathrm{d}r + \frac{4\pi}{I_0n_0}\int_0^\infty r^2|E_0|^2\frac{\partial\phi}{\partial r}\mathrm{d}r. \quad (23)$$

Using Eqs. (4), (6) and (19) in Eq. (23), we obtain the evolution equation for beam width of the laser beam, i.e., Eq. (8).

Now, using the procedure of Lam and Lipman one can obtain the equation for the evolution of the beam width as

$$\frac{\mathrm{d}^2f}{\mathrm{d}\xi^2} = \frac{1+\mathrm{e}^{-b^2}(1-b^2)}{2(1+b^2)}\frac{1}{f^3}-\left(\frac{\omega_0^2r_0^2}{c^2}\right)\times\left(\frac{\mathrm{e}^{-b^2}}{1+b^2}\right)\left[\frac{2n_2E_{00}^2}{f^3}(J_1-bJ_2)-4\frac{n_4^0E_{00}^4}{f^5}\mathrm{e}^{-a'^2(\xi-d')^2}(J_3-bJ_4)\right], \quad (24)$$

where

$$J_1 = \int_0^\infty t^3\,\mathrm{e}^{-2t^2}\cosh^4(bt)\,\mathrm{d}t, \quad (25a)$$

$$J_2 = \int_0^\infty t^2\,\mathrm{e}^{-2t^2}\cosh^3(bt)\sinh(bt)\,\mathrm{d}t, \quad (25b)$$

$$J_3 = \int_0^\infty t^3\,\mathrm{e}^{-3t^2}\cosh^6(bt)\,\mathrm{d}t, \quad (25c)$$

$$J_4 = \int_0^\infty t^2\,\mathrm{e}^{-3t^2}\cosh^5(bt)\sinh(bt)\,\mathrm{d}t, \quad (25d)$$

$$\xi = \frac{z}{k_0r_0^2}, \quad (26)$$

$$a' = k_0r_0^2a, \quad (27)$$

$$d' = \frac{\mathrm{d}}{k_0r_0^2}, \quad (28)$$

$$t = \frac{r}{r_0f}. \quad (29)$$

In the case of an initially plane wavefront, Eq. (8) must satisfy the boundary conditions

$$f(0) = 1 \quad \text{and} \quad \frac{\mathrm{d}f}{\mathrm{d}\xi}|_{\xi=0} = 0. \quad (30)$$

3. Axial phase modulation of the breather

The modulation of the phase in a laser beam arises from variations in its axial phase distribution, caused by the beam's finite spatial extent. This spatial restriction acts somewhat like a confining force, maintaining the beam's profile within defined boundaries. According to the principles of wave mechanics, limiting the beam's position inherently broadens its transverse momentum spectrum,[33] which affects the effective propagation characteristics. This interplay between confinement and momentum dispersion alters the beam's wavefront curvature, inducing a continuous phase evolution as it travels through space.

The spectral range σ_k of the breather is derived from the variance of the spectral components as[34]

$$\sigma_k = \sqrt{\langle k_x^2\rangle+\langle k_y^2\rangle}. \quad (31)$$

It gives the measure of the spread in the beam's spatial frequency spectrum. It quantifies the range of frequencies around the central wavelength, indicating the width of the spectrum in which the beam's intensity is significantly concentrated.

Here,

$$\langle k_x^2\rangle = \frac{\int_{-\infty}^\infty\int_{-\infty}^\infty k_x^2S(k_x,k_y)S^*(k_x,k_y)\,\mathrm{d}k_x\mathrm{d}k_y}{\int_{-\infty}^\infty\int_{-\infty}^\infty S(k_x,k_y)S^*(k_x,k_y)\,\mathrm{d}k_x\mathrm{d}k_y}, \quad (32a)$$

$$\langle k_y^2\rangle = \frac{\int_{-\infty}^\infty\int_{-\infty}^\infty k_y^2S(k_x,k_y)S^*(k_x,k_y)\,\mathrm{d}k_x\mathrm{d}k_y}{\int_{-\infty}^\infty\int_{-\infty}^\infty S(k_x,k_y)S^*(k_x,k_y)\,\mathrm{d}k_x\mathrm{d}k_y}, \quad (32b)$$

$$S(k_x,k_y) = \frac{1}{2\pi}\int_{-\infty}^\infty\int_{-\infty}^\infty E_0(r,z)$$

$$\times \mathrm{e}^{-\mathrm{i}r\left(k_x\cos(\theta)+k_y\sin(\theta)\right)} r\mathrm{d}r\mathrm{d}\theta. \tag{33}$$

The wave number k_0 of the laser beam is connected to transverse and longitudinal components through

$$k_0^2 = k_x^2 + k_y^2 + k_z^2. \tag{34}$$

Here, k_z denotes the axial wave number, while k_x and k_y represent the transverse wave numbers in the respective directions. The effective axial propagation constant of the optical beam is defined in the root-mean-square (rms) sense as

$$\bar{k}_z = \frac{\langle K_z^2\rangle}{k_0} = k_0 - \frac{\langle x_x^2\rangle}{k_0} - \frac{\langle k_y^2\rangle}{k_0}. \tag{35}$$

The overall on-axis phase $\theta(z)$ is connected to the effective propagation constant through the relation

$$\bar{k}_z = \frac{\partial\theta}{\partial z}. \tag{36}$$

In Eq. (35), the first term represents the phase component k_0, corresponding to an infinitely propagating plane wave along the z-axis. The second term, however, reflects the phase shift introduced by the finite beam, distinguishing it from the infinite plane wave. Thus, the axial phase shift of the laser beam can be written as

$$\frac{\mathrm{d}\theta_\mathrm{p}}{\mathrm{d}z} = -\frac{1}{k_0}\left(\langle k_x^2\rangle + \langle k_y^2\rangle\right). \tag{37}$$

Using the transformation given by Eq. (26), we obtain

$$\frac{\mathrm{d}\theta_\mathrm{p}}{\mathrm{d}\xi} = -r_0^2\left(\langle k_x^2\rangle + \langle k_y^2\rangle\right). \tag{38}$$

4. Results and discussion

In the current study, Eqs. (24) and (38) have been solved numerically using the following set of parameters: $\omega_0 = 1.13\times10^{14}$ rad/s, $r_0 = 4.6$ μm, $n_0 = 1.88$, $n_2 = 2.2\times10^{-16}$ m^2/W, $n_4^0/n_2^2 = 0.1$; $n_2E_{00}^2 = 3$; $b = (0, 0.5, 0.75, 1.1, 1.2, 1.3)$; $d' = (5, 5.5, 6)$ and $a'^2 = (0.03, 0.04, 0.05)$.

It is worth noting that the parameters used in this study are chosen solely for the numerical illustration of the derived equations. However, the presented analysis remains valid for any other set of parameters.

Figure 1 presents the variation of the dimensionless beam width $f(\xi)$ of the ChG laser beam in CQ media as a function of the dimensionless longitudinal coordinate ξ, comparing two scenarios: one with and one without a spatially modulated (hump-shaped) quintic nonlinearity. The blue curve corresponds to the evolution of the breather soliton without the hump, while the green curve illustrates the behavior with the hump-shaped quintic profile. The analysis demonstrates a distinct oscillatory evolution in the beam profile, marked by periodic contractions and expansions along the propagation axis. This behavior is rooted in the competition between nonlinear mechanisms; the third-order (cubic) component enhances beam confinement, while the fifth-order (quintic) response counteracts this by spreading the beam. At the onset, the beam intensity is relatively low, allowing the self-focusing effect to dominate and reduce the beam's transverse size. As the optical field strengthens further into the medium, the defocusing influence from the negative quintic term becomes substantial, resulting in a broadening of the beam. This dynamic balance between compression and expansion inhibits catastrophic focusing and establishes a recurring modulation in beam width. These sustained and rhythmic variations are indicative of a nonlinear wave phenomenon known as a breather soliton.

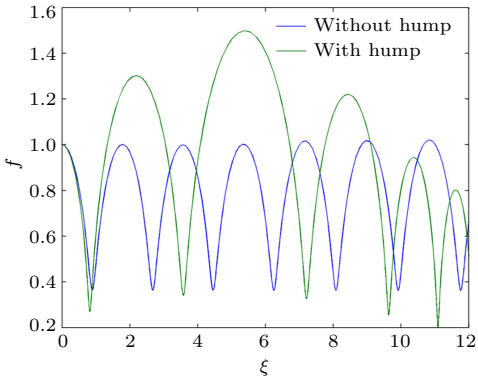


Fig. 1. Evolution of the beam width of a ChG laser beam propagating in a CQ medium, shown for cases with (green curve) and without (blue curve) a hump-shaped modulation of the quintic nonlinearity. Parameters used are $b = 0.5$, $a'^2 = 0.03$ and $d' = 5$.

It can also be seen that in the absence of the hump, the amplitude profile of the breather remains relatively stable with moderate oscillations, indicative of a quasi-stationary breather supported by the underlying cubic–quintic nonlinearity. However, when the quintic nonlinearity is axially modulated to possess a localized hump (i.e., enhanced nonlinearity in a spatial region), the amplitude of the breather significantly increases in certain intervals of ξ, particularly around the central region. Notably, the peak value of $f(\xi)$ with the hump reaches approximately 1.5, as opposed to the 1.0 limit without the hump. This implies that the hump-shaped nonlinearity acts as a nonlinear gain region, amplifying the breather soliton spatially. The envelope of the breather also exhibits more pronounced periodic modulation in the presence of the hump, confirming that the modulated quintic term introduces additional dynamic instabilities or resonance effects, which are otherwise suppressed in the uniform medium.

Figure 2 illustrates the evolution of the spot size of the laser beam through CQ media for different values of shape parameter b. The upper panel in this figure shows the variation of the beam width, whereas the lower panel shows the actual surface of the beam inside the medium. Figure 2 illustrates

that as the shape parameter b is increased within the interval $0 < b < 1$, the amplitude of the beam's breathing dynamics — reflected in its periodic expansion and contraction — becomes significantly larger. This enhancement arises because a higher b value broadens and flattens the transverse intensity profile, diverging from the sharply peaked form typical of a Gaussian beam. Such a flatter distribution interacts with a wider region of the nonlinear medium, thereby increasing the spatial domain over which nonlinear effects occur. In a cubic–quintic medium, the cubic component governing self-focusing becomes more pronounced across this extended area, which intensifies the beam's oscillatory width variations. In addition, the broader central region helps to mitigate diffraction by preserving a nearly uniform phase front, enabling the beam to stay more localized over longer propagation distances. The combined effect of stronger nonlinear coupling and reduced diffraction thus leads to a more pronounced and stable breathing pattern. Consequently, the observed rise in breathing amplitude with increasing b for $b < 1$ stems from the enhanced spatial overlap between the beam and the nonlinear medium, which amplifies self-focusing while simultaneously stabilizing the propagation dynamics.

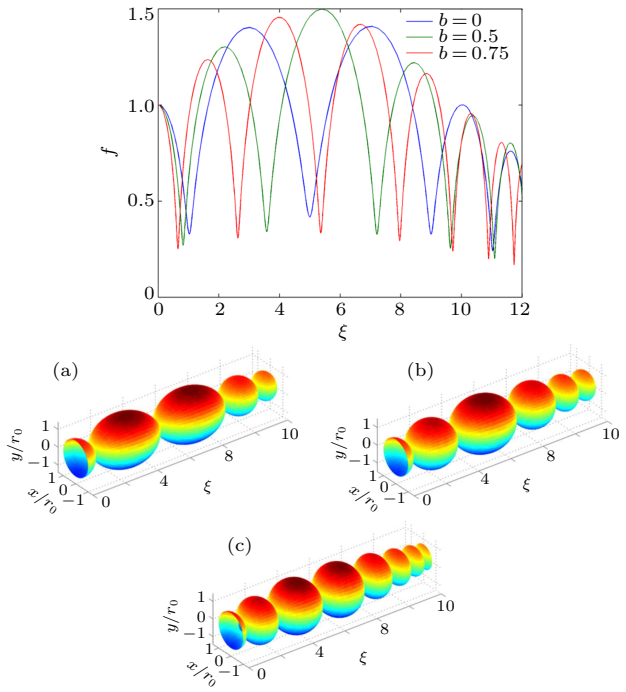


Fig. 2. Beam-width evolution of a ChG laser beam propagating in a CQ nonlinear medium with a hump-shaped modulation of the quintic nonlinearity, shown for different values of the shape parameter b: $b = 0$ (blue), $b = 0.50$ (green) and $b = 0.75$ (red). Other parameters used are $a'^2 = 0.03$ and $d' = 5$.

Figure 3 illustrates that when the shape parameter b exceeds unity, the self-focusing tendency of the cosh–Gaussian beam diminishes notably. This reduction arises because, beyond this threshold, the beam's transverse intensity distribution undergoes a structural change. Instead of exhibiting a single central maximum, the on-axis intensity weakens and two off-axis lobes emerge symmetrically. As a result, the beam evolves into a split or double-peaked profile, shifting the regions of highest intensity away from the propagation axis. Since self-focusing is primarily driven by refractive index modulation induced by localized high-intensity zones, this redistribution of optical power reduces the nonlinear lensing strength along the centerline. Moreover, the lateral displacement of peak intensities causes the beam energy to be distributed over a wider area, diminishing the nonlinear interaction per unit volume. Together, these effects make the beam less susceptible to self-focusing as b increases beyond 1.

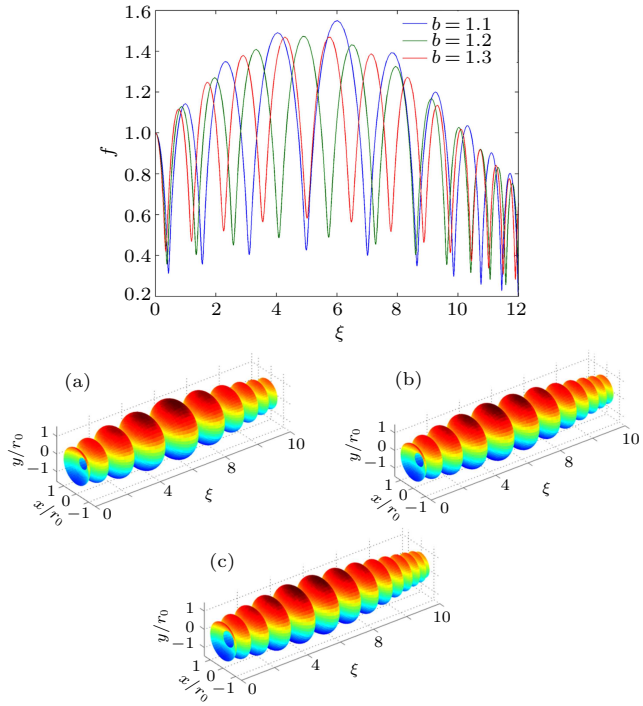


Fig. 3. Beam-width evolution of a ChG laser beam in a CQ nonlinear medium with a hump-shaped modulation of the quintic nonlinearity, plotted for different values of the shape parameter b: $b = 1.1$ (blue), $b = 1.2$ (green) and $b = 1.3$ (red). Other parameters used are $a'^2 = 0.03$ and $d' = 5$.

Figure 4 illustrates the breathing evolution of the normalized beam parameter f with propagation distance ξ for different values of the hump-width parameter a'^2. A clear trend emerges; as a'^2 increases, which results in a narrower hump-shaped quintic nonlinearity, the amplitude of the breathing oscillations becomes larger and the peaks of f rise to higher values. This indicates that when the nonlinear response is confined to a narrower spatial region, the nonlinear refractive index changes become more localized and intense, enhancing the periodic focusing–defocusing cycles.

Figure 5 presents Lyapunov exponent analysis of the beam width oscillations of the ChG laser beam for different values of the beam-shaping parameter b to examine the chaotic nature of the oscillations. Each subplot displays $\log|\Delta f(\xi)|$ in blue, with a red linear fit whose slope denotes the largest Lyapunov exponent λ. $\lambda <$ indicates a stable breather where

perturbations in the initial conditions decay and oscillations remain bounded with the propagation. $\lambda = 0$ marks the marginally stable transition. $\lambda > 0$ corresponds to the case where perturbations in the initial conditions grow with the distance of propagation. It can be seen from all the subplots that while the degree of chaos varies, all exponents remain positive, indicating that the beam propagation is consistently chaotic for all b-values shown, with no transition to regular or periodic behavior. This indicates that the beam trajectory in phase space is sensitive to initial conditions. For the beam width, this manifests as irregular oscillations around an average value — the width continues to breathe, but neither stabilizes to a single periodic cycle nor collapses completely. The CQ medium with hump-shaped quintic nonlinearity acts as a continuous perturbing mechanism, preventing the system from ever reaching a perfectly periodic or stationary state.

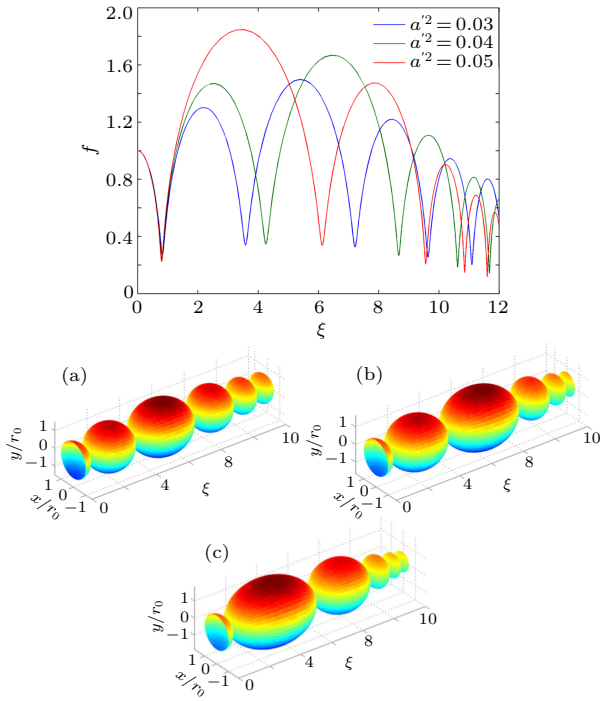


Fig. 4. Beam-width evolution of a ChG laser beam propagating in a CQ nonlinear medium with a hump-shaped modulation of the quintic nonlinearity, shown for different values of the parameter a': $a' = 0.03$ (blue), $a' = 0.04$ (green) and $a' = 0.05$ (red). Other parameters used are $b = 0.5$ and $d' = 5$.

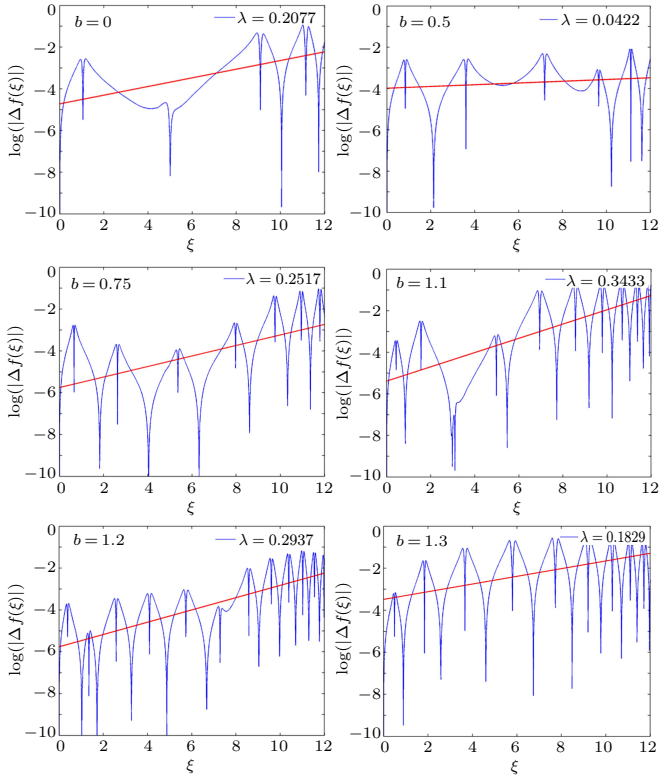


Fig. 5. Lyapunov exponent analysis of beam-width oscillations of a ChG laser beam for varying values of the shape parameter b, evaluated at fixed $a'^2 = 0.03$ and $d' = 5$.

Figure 6 displays the evolution of the axial phase modulation (θ_p) versus the normalized propagation distance (ξ) for a ChG laser beam in a CQ nonlinear medium, which reveals the characteristic breathing dynamics of a spatial breather soliton. The negative values of θ_p represent a cumulative phase delay or a Gouy-like phase shift acquired by the self-focused beam as it propagates. The oscillatory nature of both curves signifies the beam's breather-soliton formation, where its beam width periodically contracts (self-focusing) and expands (self-defocusing) as it moves through the medium, and this change in width directly modulates the axial phase. The key comparison is between the "without hump" (blue line) and "with hump" (green line) scenarios for the quintic nonlinearity profile. The "with hump" case (green) results in a reduced magnitude of the total phase delay and milder oscillations compared to the "without hump" case (blue). This suggests that the hump-shaped quintic nonlinearity introduces a stronger effective stabilizing or defocusing component that better counteracts the cubic (Kerr) self-focusing, leading to a more controlled and less intense breathing cycle with a slower overall accumulation of the nonlinear phase shift.

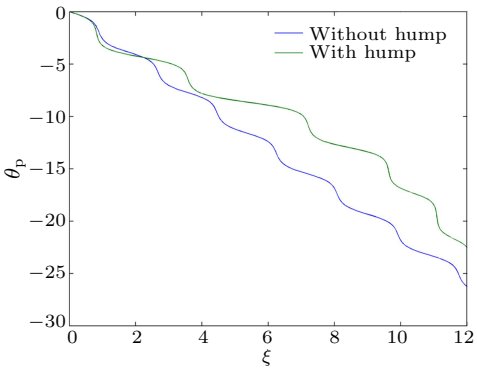


Fig. 6. Axial phase evolution of a breather in a CQ nonlinear medium, comparing the cases with (green) and without (blue) a hump-shaped modulation of the quintic nonlinearity. Parameters used are $b = 0.5$, $a'^2 = 0.03$ and $d' = 5$.

The graph from Figs. 7 and 8 illustrates a crucial dependence of the axial phase modulation (θ_p) on the beam's shape parameter (b), highlighting a complex interplay between the initial beam profile and the resulting nonlinear axial phase shift. For small values of b ($b < 1$), the beam profile, which

transitions from a Gaussian ($b = 0$) to a slightly flattened-top shape, directs more power towards the center, enhancing the effective self-focusing of the cubic nonlinearity. This enhanced compression leads to a faster accumulation of the negative axial phase delay (a steeper $\left|\mathrm{d}\theta_\mathrm{p}/\mathrm{d}\xi\right|$ slope). However, as b increases past the critical point ($b > 1$), the profile transforms into a distinct dark-hollow beam, shifting the high-intensity rings significantly off the beam axis. This on-axis intensity depletion weakens the central self-focusing force, allowing the inherent diffraction to partially dominate the dynamics. Consequently, the beam's ability to compress is reduced, resulting in a slower rate of phase accumulation (a gentler $\left|\mathrm{d}\theta_\mathrm{p}/\mathrm{d}\xi\right|$ slope). This transition demonstrates that the shape parameter b acts as a geometrical switch that fundamentally controls the competition between diffraction and nonlinearity, directly dictating the strength and rapidity of the breather soliton's self-compression and, thus, the evolution of the nonlinear phase.

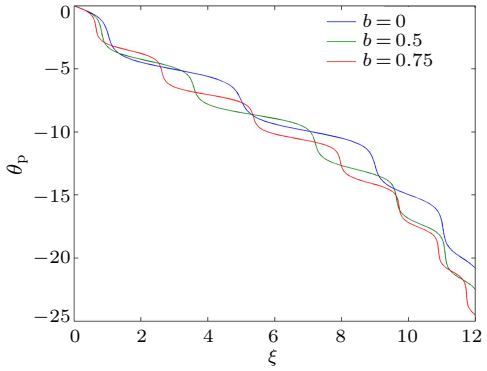


Fig. 7. Axial phase evolution of a ChG laser beam propagating in a CQ nonlinear medium with a hump-shaped modulation of the quintic nonlinearity, shown for different values of the shape parameter b: $b = 0$ (blue), $b = 0.50$ (green) and $b = 0.75$ (red). Other parameters used are $a'^2 = 0.03$ and $d' = 5$.

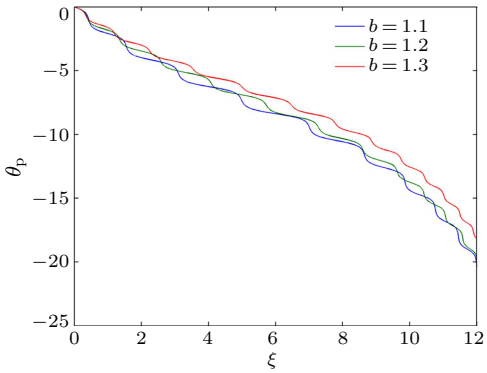


Fig. 8. Axial phase evolution of a ChG laser beam propagating in a CQ nonlinear medium with a hump-shaped modulation of the quintic nonlinearity, shown for different values of the shape parameter b: $b = 1.1$ (blue), $b = 1.2$ (green) and $b = 1.3$ (red). Other parameters used are $a'^2 = 0.03$ and $d' = 5$.

Figure 9 illustrates how the axial phase accumulated by the spatial breather soliton is controlled by the nonlinear medium's profile. It can be seen that the parameter a'^2, which is inversely related to the width of the quintic hump, demonstrates that increasing a'^2 (narrower hump) leads to a less negative, more stable phase evolution (red line), which counter-intuitively implies that a narrower hump results in a stronger overall stabilization/defocusing of the breather, thereby limiting the beam's self-compression and the resulting nonlinear phase accumulation.

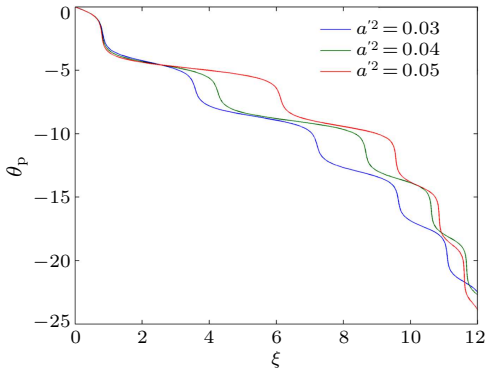


Fig. 9. Axial phase evolution of a ChG laser beam in a CQ nonlinear medium with a hump-shaped modulation of the quintic nonlinearity, shown for different values of the parameter a'^2: $a'^2 = 0.03$ (blue), 0.04 (green) and 0.05 (red). Other parameters used are $b = 0.5$ and $d' = 5$.

5. Conclusion

We have presented a detailed theoretical investigation into the nonlinear propagation and breather soliton formation of a ChG laser beam in a medium characterized by a CQ nonlinearity with a spatially modulated hump-shaped quintic term. Employing the moment method, we derived a set of coupled evolution equations for the beam's width and axial phase modulation (θ_p) that successfully captured the characteristic periodic breathing dynamics of the spatial breather soliton.

Our results underscore the crucial role of both the input beam profile and the quintic nonlinearity's spatial characteristics in governing the propagation. The axial phase modulation, which represents the nonlinear Gouy phase shift, was shown to be highly sensitive to the controlling parameters.

Quintic hump profile The comparison between the "without hump" and "with hump" scenarios (Fig. 1) revealed that the hump introduces a stronger effective stabilization. This counteracts the cubic self-focusing, resulting in a reduced magnitude of the accumulated phase delay (θ_p) and milder oscillations.

Beam shape parameter (b) The decentered parameter b was found to control the intensity of the breathing. For $b < 1$, increasing b initially enhances self-focusing, leading to a faster drop in the axial phase. However, for $b > 1$, the transition to a dark-hollow profile weakens central focusing, thereby slowing the phase decrease.

Hump width (a'^2) Increasing a'^2 (corresponding to a narrower hump) led to a stronger suppression of the phase delay and breathing intensity, suggesting that a more localized concentration of the quintic term is more effective at stabilizing the beam.

In summary, these findings demonstrate that the combination of the unique cosh–Gaussian profile and the engineered hump-shaped quintic nonlinearity offers a versatile platform for the tunable generation and precise control of spatial breathers. The ability to manage the nonlinear phase accumulation and breathing frequency through parameters such as b and d' is vital for potential applications in all-optical switching, controlled energy delivery, and high-intensity beam manipulation.

References

[1] Simmons W, Hunt J and Warren W 1981 *IEEE J. Quantum Electron.* **17** 1727
[2] Wiersma N, Marsal N, Sciamanna M and Wolfersberger D 2014 *Opt. Lett.* **39** 5997
[3] Busschaert S, Flöry N, Papadopoulos S, Parzefall M, Heeg S and Novotny L 2019 *Nano Lett.* **19** 6097
[4] Geng W, Fang Y, Wang Y, Bao C, Liu W, Pan Z and Yue Y 2024 *Nanophotonics* **13** 3253
[5] Segev M and Stegeman G 1998 *Phys. Today* **51** 42
[6] Herman R 1992 *Am. Sci.* **80** 350
[7] Stegeman G I and Segev M 1999 *Science* **286** 1518
[8] Stix G 2001 *Sci. Am.* **285** 30
[9] Alberucci A, Jisha C P and Assanto G 2016 *J. Opt.* **18** 125501
[10] Li L, Yan Y and Xie Y 2021 *Optik* **246** 167713
[11] Dabby F W and Whinnery J R 1968 *Appl. Phys. Lett.* **13** 284
[12] Akhmanov S A, Sukhorukov A P and Khokhlov R V 1968 *Sov. Phys. Usp.* **10** 609
[13] Chabchoub A, Kibler B, Dudley J M and Akhmediev N 2014 *Philos. Trans. R. Soc. A* **372** 20140005
[14] Yolbarsop A, Porcelli F, Banerjee D, Kim C C and Hong L 2023 *Phys. Lett. A* **479** 128940
[15] Matuszewski M, Infeld E, Rowlands G and Trippenbach M 2005 *Proc. R. Soc. A* **461** 3561
[16] Kawaguchi S 2022 *Adv. Math. Phys.* **2022** 1637071
[17] Karlsson M, Anderson D and Desaix M 1992 *Opt. Lett.* **17** 22
[18] Kelley P L 1965 *Phys. Rev. Lett.* **15** 1005
[19] Biswas A 2003 *Opt. Commun.* **216** 427
[20] Pushkarov D and Tanev S 1996 *Opt. Commun.* **124** 354
[21] Lü B, Ma H and Zhang B 1999 *Opt. Commun.* **164** 165
[22] Eyyuboğlu H T and Baykal Y 2005 *Appl. Opt.* **44** 976
[23] Gupta N, Kumar S, Gnaneshwaran A, Kumar S and Choudhry S 2021 *J. Opt.* **50** 701
[24] Habibi M and Ghamari F 2015 *IEEE Trans. Plasma Sci.* **43** 2160
[25] Kartashov Y V, Malomed B A and Torner L 2011 *Rev. Mod. Phys.* **83** 247
[26] Zhong Y, Triki H and Zhou Q 2024 *Chin. Phys. Lett.* **41** 070501
[27] Zhong Y, Yang D F, Liu Y X, Li J, Triki H and Zhou Q 2025 *Chin. Phys. Lett.* **42** 080002
[28] Rosencher E, Fiore A, Vinter B, Berger V, Bois P and Nagle J 1996 *Science* **271** 168
[29] Paré C and Bélanger P A 1992 *Opt. Quantum Electron.* **24** 1051
[30] Sodha M S, Sinha S K and Sharma R P 1979 *J. Phys. D: Appl. Phys.* **12** 1079
[31] Lam J F, Lippmann B and Tappert F 1975 *Opt. Commun.* **15** 419
[32] Lam J F, Lippmann B and Tappert F 1977 *Phys. Fluids* **20** 1176
[33] Hariharan P and Robinson P A 1996 *J. Mod. Opt.* **43** 219
[34] Feng S and Winful H G 2001 *Opt. Lett.* **26** 485